AD-A147 847 INTENSITY VECTORS OF SOUND SCATTERING BY A SPHERICAL SHELL(U) ADMIRALTY MARINE TECHNOLOGY ESTABLISHMENT TEDDINGTON (ENGLAND) J H JAMES JUL 84 AMTE(N)/TM84080 1/1

UNCLASSIFIED DRIC-BR-93176 F/G 20/1 NL

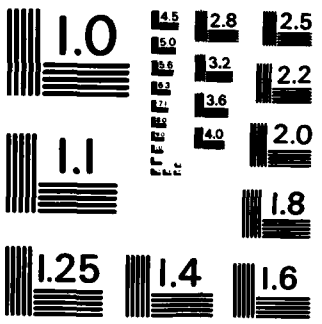

MICROCOPY RESOLUTION TEST CHART
NATIONAL BUREAU OF STANDARDS-1963-A

UNLIMITED

DR93176

TECH MEMO AMTE(N)TM84080

COPY No 16

ADMIRALTY MARINE TECHNOLOGY ESTABLISHMENT

AD-A147 847

INTENSITY VECTORS OF SOUND SCATTERING BY A SPHERICAL SHELL

J. H. JAMES

AMTE (Teddington)
Queen's Road TEDDINGTON
Middlesex TW11 0LN

JULY 1984

AMTE(N)TM84080

UNLIMITED

INTENSITY VECTORS OF SOUND SCATTERING BY A SPHERICAL SHELL

BY

J H JAMES

cont 4 p 3

SUMMARY

Mathematical formulae are given from which target strength spectra and acoustic intensity vectors are calculated. The excitation is a time-harmonic plane wave. Intensity vector plots show the considerable distortion of the incident sound field that may be present when an elastic scatterer is excited at a resonant frequency.

AMTE (Teddington)
Queen's Road
TEDDINGTON Middx TW11 OLN

20 pages
8 figures

July 1984

1. INTRODUCTION

The dynamics and acoustics of a uniform spherical shell is a basic problem in the field of fluid-structure interaction because the relative simplicity of the geometry and equations enables closed-form solutions in terms of series of Legendre polynomials and spherical Bessel functions, thus rendering possible general insight into the effect of fluid loading on the dynamics of non-planar elastic surfaces. Additionally, numerical results may be used as a check of the correctness of computer programs based on purely numerical formulations such as the coupled finite element and Helmholtz integral equation methods. Much of the theoretical work on the dynamics and acoustics of a thin spherical shell is contained in the standard text [1] on fluid-structure interaction. Wong & Hayek [2] have analysed, both analytically and experimentally, the vibration and acoustic radiation from point force excited shells in air and in water. They found good agreement between the resonant frequencies determined by theory and experiment. Other references of interest are contained in the locations cited.

Acoustic intensity vector plots can illustrate vividly the power flow in an acoustic fluid. Spicer's plots [3] show the subsonic and 'leaky' waves associated with the interaction between an elastic plate and a fluid when the former is driven by a time-harmonic force. James [4] gives vector plots which show that there may be significant interchange of power between a duct's wall and its contained fluid when the excitation is a force. Intensity vector plots of the scattered sound field due to plane wave excitation of an infinite fluid-filled cylindrical shell have been given by James [5]. Vector plots of the total sound field were also obtained but not reported. The plots did not show significant distortion of the incident wave, except for the special case of a pressure release scatterer, possibly because there was no marked resonant response of the shell.

It is the main purpose of this memorandum to examine, by means of acoustic intensity vector plots, the distortion of the incident sound field due to the presence of a spherical shell whose target strength spectrum contains well-defined resonant peaks. The mathematics is given in Section 2 with a minimum of explanation because most of it can be found scattered throughout the standard text [1]. Target-strength spectra and vector plots obtained from Fortran programs are discussed in Section 3.

2. MATHEMATICS OF PROBLEM

(a) Shell Dynamics

The radial and tangential displacements at the shell's surface are expressed as a series of Legendre polynomials of argument $\mu = \cos\theta$, viz.

$$U(\theta) = \sum_{n=0}^{\infty} (1-\mu^2)^{1/2} U_n P_n'(\mu) \qquad (1)$$

$$W(\theta) = \sum_{n=0}^{\infty} W_n P_n(\mu) \qquad (2)$$

whose amplitudes U_n and W_n are obtained from the matrix relation

$$\begin{bmatrix} a_{11} & a_{12} \\ a_{21} & a_{22} \end{bmatrix} \begin{bmatrix} U_n \\ W_n \end{bmatrix} = \begin{bmatrix} 0 \\ P_n \end{bmatrix} \tag{3}$$

where, for coupled membrane and bending theory in which effects due to rotary inertia and transverse shear are neglected,

$$\begin{aligned} a_{11} &= E_1(1+\beta^2)(\nu+\lambda_n-1) - \omega^2\rho_s h \\ a_{12} &= E_1\beta^2(\nu+\lambda_n-1) + E_1(1+\nu) \\ a_{21} &= \lambda_n a_{12} \\ a_{22} &= E_1\beta^2\lambda_n(\nu+\lambda_n-1) + 2E_1(1+\nu) - \omega^2\rho_s h \\ &\quad + \rho_2 c_2 \omega\, h_n(k_2a)/h_n'(k_2a) - \rho_1 c_1 \omega j_n(k_1a)/j_n'(k_1a) \end{aligned} \tag{4}$$

In the above, h is the shell's thickness and a is its mean radius; $E_1=Eh/[(1-\nu^2)a^2]$ where E is Young's modulus and ν is Poisson's ratio; $\beta^2 = h^2/12a^2$ and $\lambda_n = n(n+1)$; ρ_s is the density of the shell's material, and ρ_1 and ρ_2 are the densities of the interior and exterior fluids whose sound velocities are c_1 and c_2, respectively; k_1 and k_2 are acoustic wave numbers, ω/c_1 and ω/c_2; j_n and h_n are spherical Bessel functions, and P_n are Legendre polynomials of degree n; the prime on various quantities denotes differentiation with respect to their arguments. The time-harmonic factor, $\exp(-i\omega t)$, will be omitted throughout. The geometry of the problem is shown in Figure 1, in which it is evident that the problem is axisymmetric, i.e. in a system of spherical coordinates (R,θ,ϕ) the displacements are independent of the circumferential angle ϕ.

(b) Excitation

In equation (3) F_n are the coefficients of the Legendre series expansion of the excitation stress

$$F(\theta) = \sum_{n=0}^{\infty} F_n P_n(\mu) \tag{5}$$

For the special case of acoustic excitation

$$F(\theta) = -[p_i(R,\theta) + p_r(R,\theta)]_{R=a} \tag{6}$$

where

$$p_i(R,\theta) = P_i \exp(ik_2 R.\cos\theta)$$

$$= P_i \sum_{n=0}^{\infty} (2n+1) i^n P_n(\cos\theta) j_n(k_2 R) \tag{7}$$

is the acoustic pressure due to the incident plane wave and

$$p_r(R,\theta) = -P_i \sum_{n=0}^{\infty} (2n+1) i^n P_n(\cos\theta) j_n'(k_2 a) h_n(k_2 R)/h_n'(k_2 a) \tag{8}$$

is the pressure scattered by the shell behaving as a rigid immovable body.

Combining equations (7) and (8), with the help of the Wronskian relation, $j_n(x)y'_n(x) - j'_n(x)y_n(x) = 1/x^2$, gives the excitation as

$$F_n = -(P_i/k_2^2 a^2)(2n+1) i^{n+1}/h_n'(k_2 a) \tag{9}$$

(c) Exterior Pressure

The pressure in the exterior fluid is the sum of three terms, viz

$$p_2(R,\theta) = p_i(R,\theta) + p_r(R,\theta) + p_e(R,\theta) \tag{10}$$

The first term, p_i, is the pressure due to the incident wave, equation (7); the second term, p_r, is the pressure scattered by the shell behaving as a rigid body, equation (8); and the third term, p_e, is the sound field arising from elastic vibrations of the shell. This term is

$$p_e(R,\theta) = \rho_2 c_2 \omega \sum_{n=0}^{\infty} W_n P_n(\cos\theta) h_n(k_2 R)/h_n'(k_2 a) \tag{11}$$

It is very easily verified that the boundary condition

$$[\partial p_2(R,\theta)/\partial R]_{R=a} = \rho_2 \omega^2 W(\theta) \tag{12}$$

which embodies continuity of normal displacement between exterior fluid and shell surface is satisfied. The effect of the interior fluid is completely

described by the term $\rho_1 c_1 \omega j_n(k_1 a)/\dot{j}_n(k_1 a)$ in the expression for the coefficient a_{22} of equation (4), whose term, $\rho_2 c_2 \omega h_n(k_2 a)/\dot{h}_n(k_2 a)$, is evidently the radiation loading of the exterior fluid.

The scattered pressure is simply

$$p_s(R,\theta) = p_r(R,\theta) + p_\theta(R,\theta) \tag{13}$$

which is put into its far-field form, p_{sf}, by replacing the spherical Hankel function by its value for a large argument, viz.,

$$h_n(k_2 R) \simeq \exp[i(k_2 R - (n+1)\pi/2)]/k_2 R \tag{14}$$

(d) Intensity Vectors

The radial and circumferential components of the time averaged exterior intensity vector of the total acoustic field are defined as

$$I_R(R,\theta) = (1/2)\mathrm{Re}[p_2(R,\theta)\dot{W}_2^*(R,\theta)]$$

$$I_\theta(R,\theta) = (1/2)\mathrm{Re}[p_2(R,\theta)\dot{U}_2^*(R,\theta)] \tag{15}$$

where * and . (= $-i\omega$) denote complex conjugate and time-differentiation, respectively. The particle displacements

$$W_2(R,\theta) = W_1(R,\theta) + W_r(R,\theta) + W_\theta(R,\theta)$$

$$U_2(R,\theta) = U_1(R,\theta) + U_r(R,\theta) + U_\theta(R,\theta) \tag{16}$$

are related to the pressure by the formulae

$$\partial p_2(R,\theta)/\partial R = \rho_2 \omega^2 W_2(R,\theta)$$

$$\partial p_2(R,\theta)/R\partial\theta = \rho_2 \omega^2 U_2(R,\theta) \tag{17}$$

Hence, from equations (10) and (16)

$$\rho_2 \omega^2 W_1(R,\theta) = ik_2 P_1 \cos\theta . \exp(ik_2 R.\cos\theta)$$

$$R\rho_2 \omega^2 U_1(R,\theta) = -ik_2 R P_1 \sin\theta . \exp(ik_2 R.\cos\theta)$$

$$\rho_2\omega^2 W_r(R,\theta) = -k_2 P_i \sum_{n=0}^{\infty} (2n+1) i^n P_n(\cos\theta) j_n'(k_2 a) h_n'(k_2 R)/h_n'(k_2 a)$$

$$R\rho_2\omega^2 U_r(R,\theta) = P_i \sin\theta \sum_{n=0}^{\infty} (2n+1) i^n P_n'(\cos\theta) j_n'(k_2 a) h_n(k_2 R)/h_n'(k_2 a) \qquad (18)$$

$$\rho_2\omega^2 W_e(R,\theta) = \rho_2 c_2 \omega k_2 \sum_{n=0}^{\infty} W_n P_n(\cos\theta) h_n'(k_2 R)/h_n'(k_2 a)$$

$$R\rho_2\omega^2 U_e(R,\theta) = -\rho_2 c_2 \omega \sin\theta \sum_{n=0}^{\infty} W_n P_n'(\cos\theta) h_n(k_2 R)/h_n'(k_2 a)$$

The magnitude and direction of the intensity vector in the XZ plane are given by the formulae

$$I = \sqrt{[I_R^2(R,\theta)+I_\theta^2(R,\theta)]}$$

$$\Phi = \theta + \arctan[I_\theta(R,\theta)/I_R(R,\theta)] \qquad (19)$$

in which $R = \sqrt{(X^2+Z^2)}$ and $\theta = \arctan(X/Z)$.

3. NUMERICAL RESULTS

(a) General

A Fortran program has been written to calculate the a target strength defined as

$$TS = 20.0 \times \log_{10}[(R/P_i)|p_{sf}(R,\theta)|]$$

where

$$p_{sf}(R,\theta) = \lim_{R\to\infty} [p_r(R,\theta) + p_e(R,\theta)]$$

is the pressure scattered to the far-field. The intensity vectors are calculated from computations of pressure and displacements close to the shell.

In Figures 2-8, the following constants in SI units were used to obtain the plotted data:

Steel shell: $E = 19.5\times10^{10}$ $\nu = 0.29$ $\rho_s = 7700.0$ $a = 1.0$
$h = 0.01/0.1$ for the thin/thick shell

Water: $\rho = 1000.0$ $c = 1500.0$

Shell damping was included in the computations by setting Young's modulus to the complex value $E(1-i\eta)$ where η, the hysteretic loss-factor, was chosen as 0.01.

(b) Target Strength Spectra

Figure 2 shows monostatic target strength spectra of the thin shell. The frequency range extends to a ka-value of 8.4. In the low frequency regime there are dominant resonant peaks which are labelled by their individual harmonic numbers. These resonances belong to the lower branch, which has no resonances at n=0 or 1, of the frequency/mode-number dispersion plot [2]. The resonant peaks of the empty shell are particularly high, the n=2 peak being almost 20dB above the 'rigid body' datum plot. Above 400Hz the smooth variation in the target strength spectra is caused by the dominance of modes which are excited at frequencies remote from their natural frequencies. In this frequency regime the plots are similar to those of sound scattering from an infinite cylindrical shell [5].

In Figure 3, which shows target strength spectra of the thick shell, the resonant peaks are broader and extend throughout the entire frequency range, their levels being up to 15dB above the 'rigid' datum plot. When the shell is filled with water there is a small peak due to an n=1 resonance, presumably of the upper branch [2] of the dispersion plot.

(c) Intensity Vectors

In Figures 4-8, which show intensity vector plots, in the Z-X plane, at selected frequencies, the plotted lengths of the vectors are proportional to $I^{1/2}$. They have been normalised, in each plot separately, to a maximum length equal to the grid spacing. Due to the symmetry of the excitation and geometry, it is only the vectors in the region $X \geq 0$ that have been plotted, the plotting region extending over the ranges $-2 \leq Z \leq 2$ and $0 \leq X \leq 2$.

In Figure 4 plots of a rigid (immovable) sphere are shown at 250 and 1000Hz. There is a minimum of distortion of the incident sound field, although the initial development of the shadow zone behind the sphere is evident at 1000Hz.

In Figure 5 the large distortion of the incident sound field at resonant frequencies of the empty thin shell is shown. At 271Hz (n=2) there is a maximum of power flow into the shell at the poles, and a maximum of power flow out of the shell at the equator. At 342Hz (n=3) there is a minimum of power flow into the shell at the poles, but still a maximum of power flow out of the shell at the equator. This behaviour is consistent with the behaviour of the Legendre polynomials P_2 and P_3.

The vector plots of the empty thin shell at 788Hz (dip in spectrum) and at 1300Hz (a maximum in spectrum) are shown in Figure 6. Unlike the previous plots which show violent distortions at resonance, these plots are much the same as the 'rigid body' plot of Figure 4B.

In Figure 7, the vector plot of the fluid-filled thin shell at the resonant frequency of 194Hz (n=2) is much the same as the plot of Figure 5A.

The vector plot of the fluid-filled thin shell at 175Hz (dip in spectrum) shows significant distortion at the equator only.

In Figure 8A, the vectors of the empty thick shell are shown at 497Hz, the resonant frequency of the n=2 mode. The most significant feature is the the intense power circulation in the illuminated region. In Figure 8B, the vectors of the fluid-filled thick shell are shown at 556Hz, the resonant frequency of the n=1 mode which is thought to belong to the upper branch of the shell dispersion relation. It is difficult to interpret these plots due to interference from neighbouring modes.

4. CONCLUDING REMARKS

The limited number of intensity vector plots shown herein have illustrated vividly the substantial distortion of the incident sound field that may take place when a system is excited at a resonant frequency, which is defined as a frequency at which there is a sharp maximum in the target strength spectra. Due to the importance of the sphere as a standard target for underwater reflectivity measurements, the following follow-up projects may be of some value:

(i) Development of Fortran program for predicting target stength and intensity vectors of a sphere composed of an arbitrary number of layers of elastic solids and fluids. Skelton's work on layered cylinders [6] is of relevance here.

(ii) Investigation of sound scattering by a fluid-filled spherical shell with point attachments such as masses and springs. The method of dynamic stiffness coupling as used by, for example, Spicer [3] enables the point attachments to be treated as forces of constraint.

J.H.JAMES (PSO)

REFERENCES

1. JUNGER M., FEIT D., Sound Structures and their Interaction, MIT Press 1972.

2. WONG E.H., HAYEK S.I., Vibration and acoustic radiation from point excited spherical shells, The Shock & Vibration Bulletin, No.52 Part 5, May 1982, pages 135-148.

3. SPICER W.J., Acoustic intensity vectors from an infinite plate with line attachments, Admiralty Marine Technology Establishment, Teddington, AMTE(N)TM81086, October 1981.

4. JAMES J.H., Fluid layer between infinite elastic plates: I. Mathematics and intensity vectors, Admiralty Marine Technology Establishment, Teddington, AMTE(N)TM84053, February 1984.

5. JAMES J.H., Sound scattering from infinite fluid-filled cylindrical shell, Admiralty Marine Technology Establishment, Teddington, AMTE(N)TM83107, October 1983.

6. SKELTON E.A., Sound radiation from a cylindrical pipe composed of cylindrical layers of fluids and elastic solids, Admiralty Marine Technology Establishment, Teddington, AMTE(N)TM83007, January 1983.

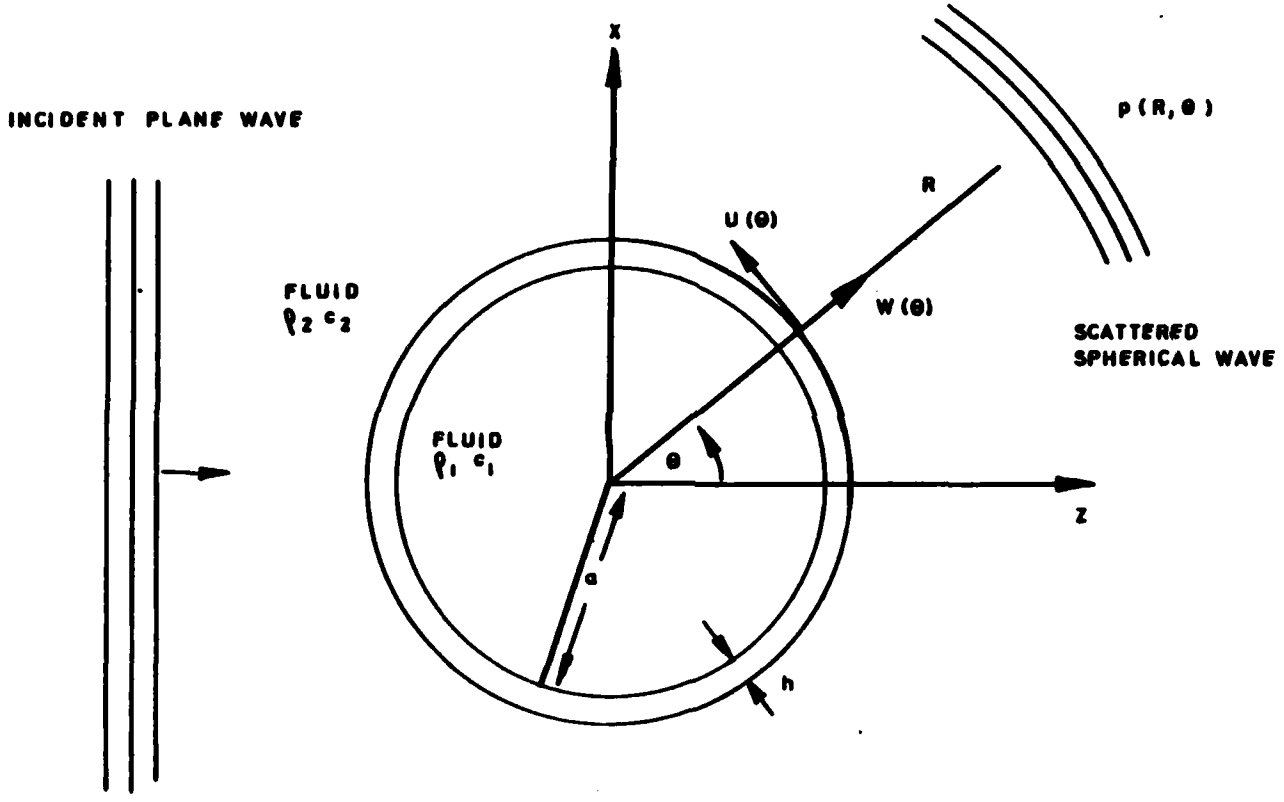

FIG. 1 SOUND SCATTERING FROM SPHERICAL SHELL

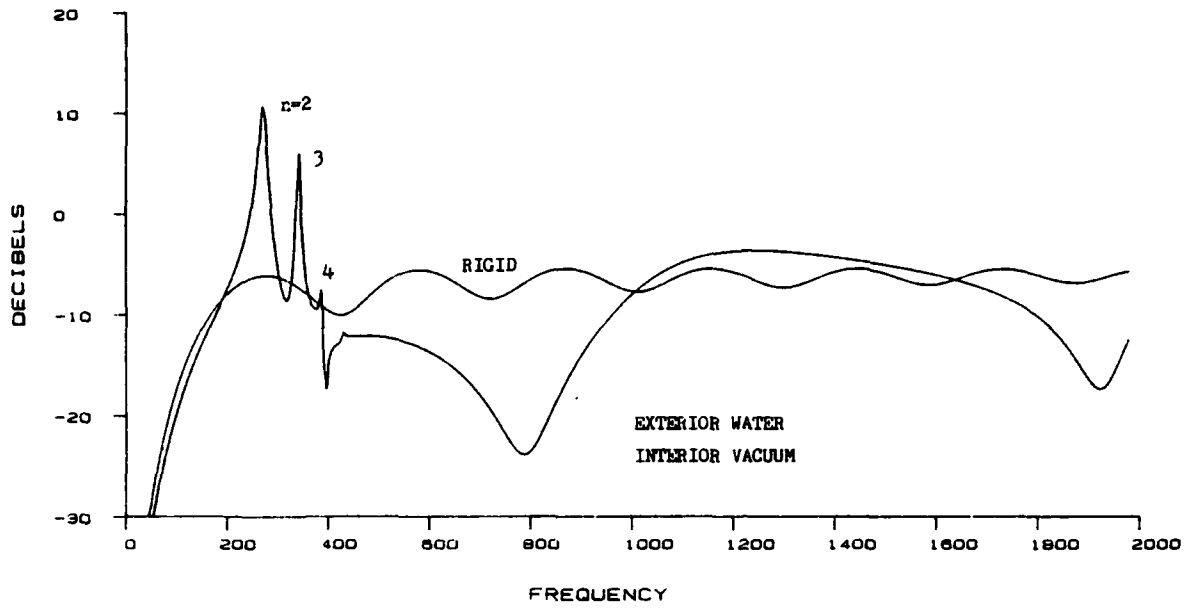

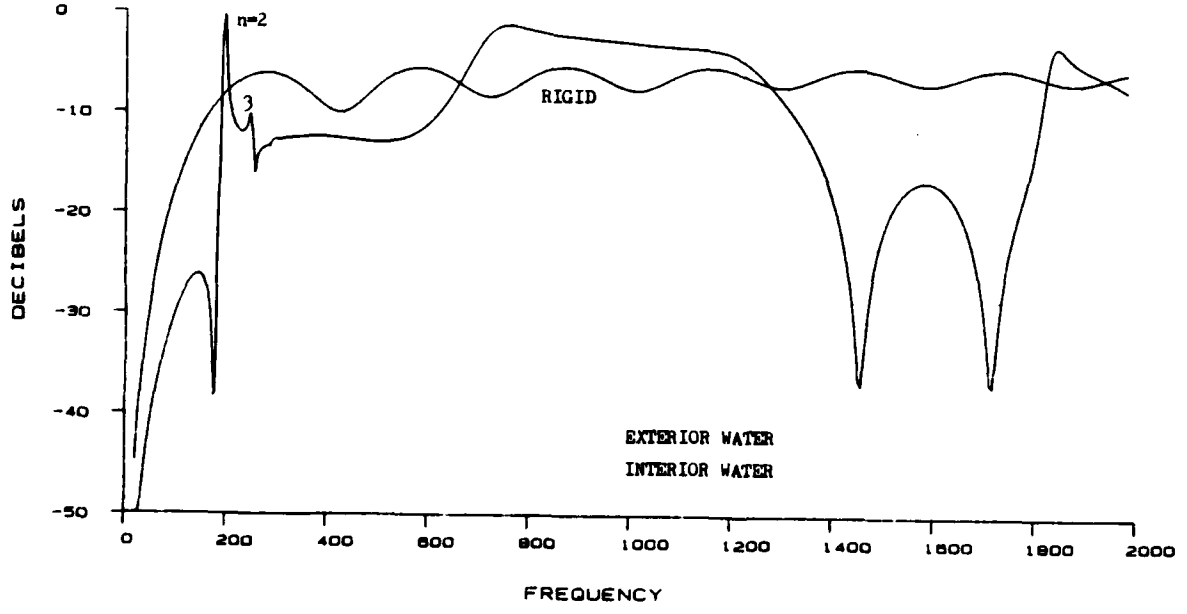

FIG.2 MONOSTATIC TARGET STRENGTH OF THIN SHELL

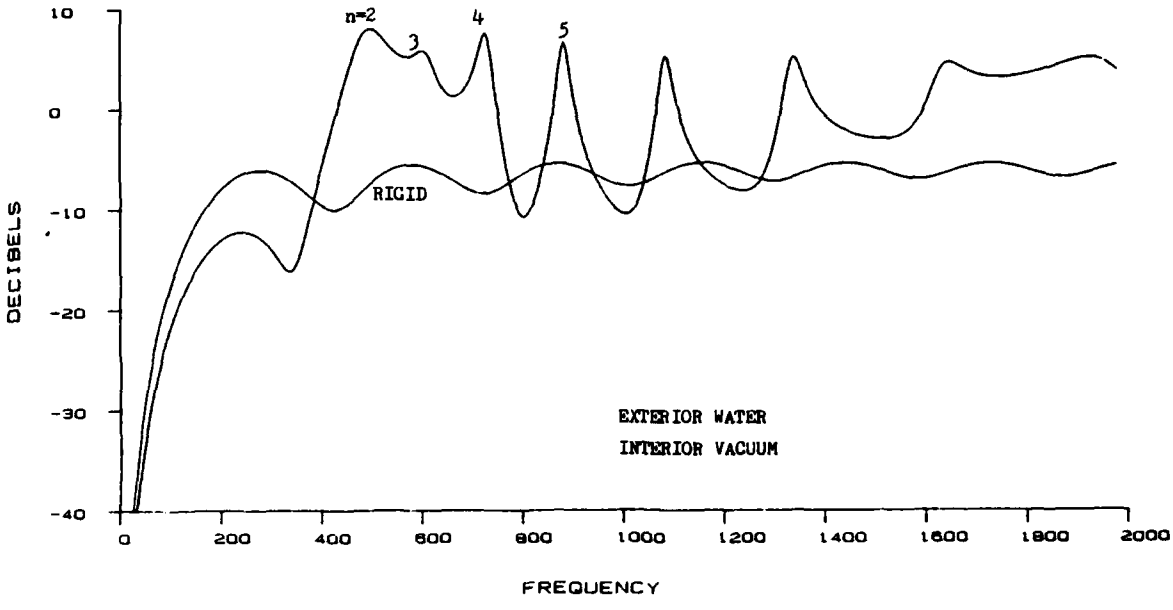

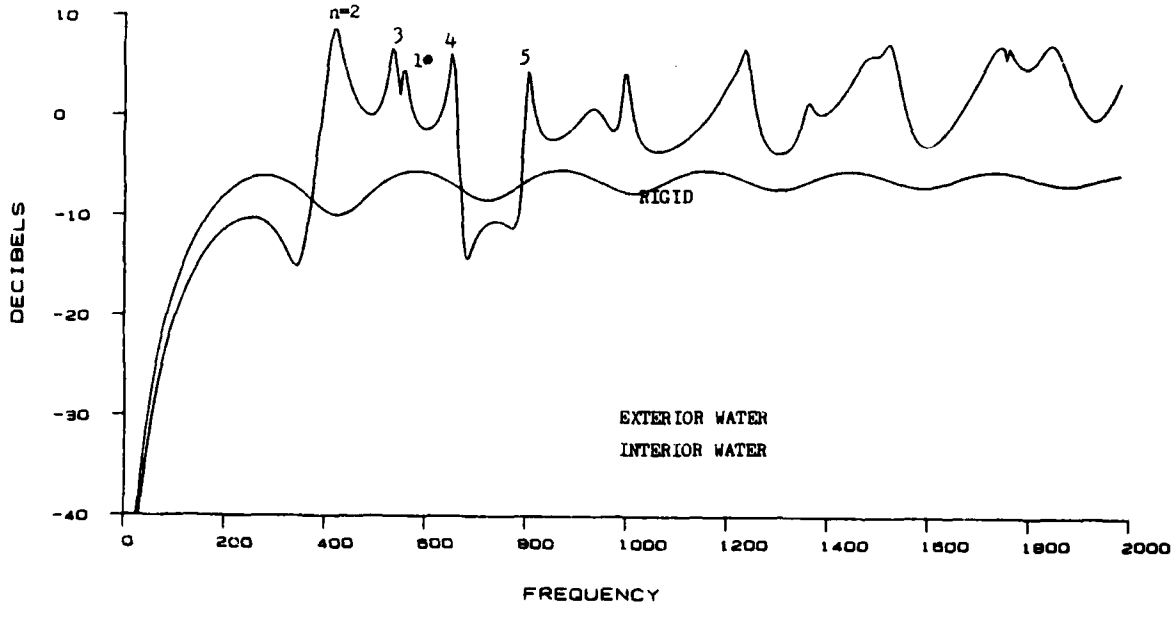

FIG.3 MONOSTATIC TARGET STRENGTH OF THICK SHELL

A. FREQUENCY = 250Hz

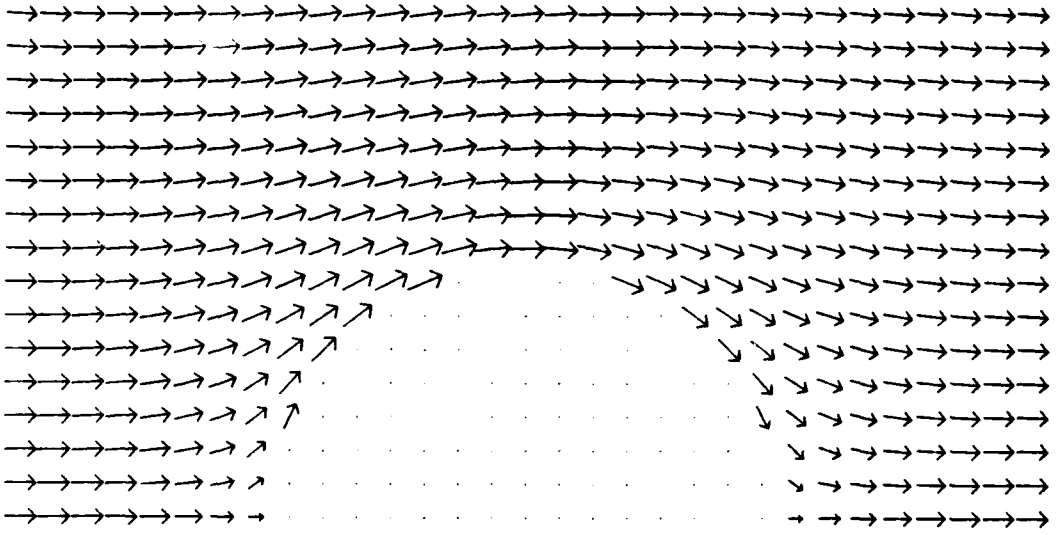

B. FREQUENCY = 1000Hz

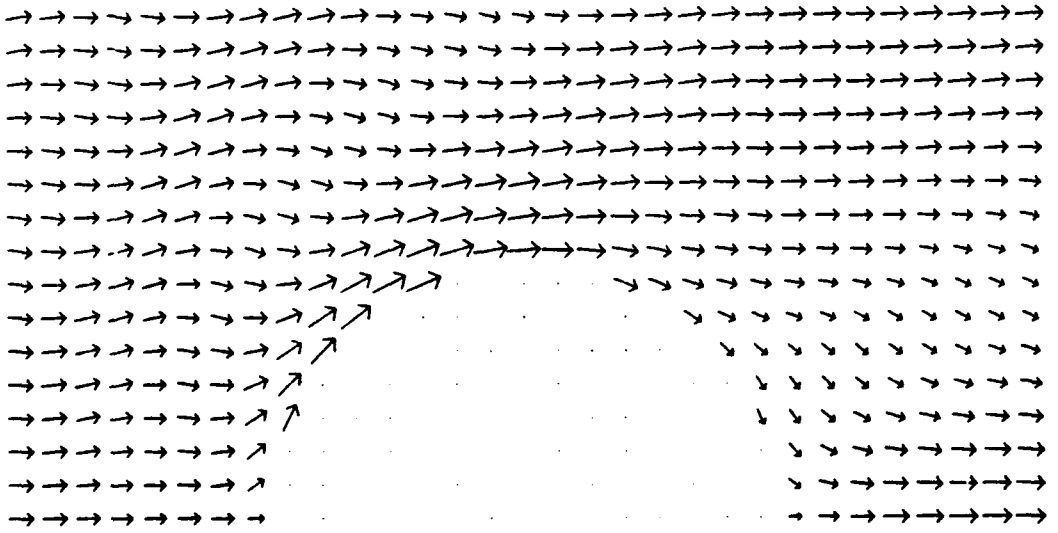

FIG.4 INTENSITY VECTORS OF RIGID SPHERE

A. FREQUENCY = 271Hz (n=2 resonance)

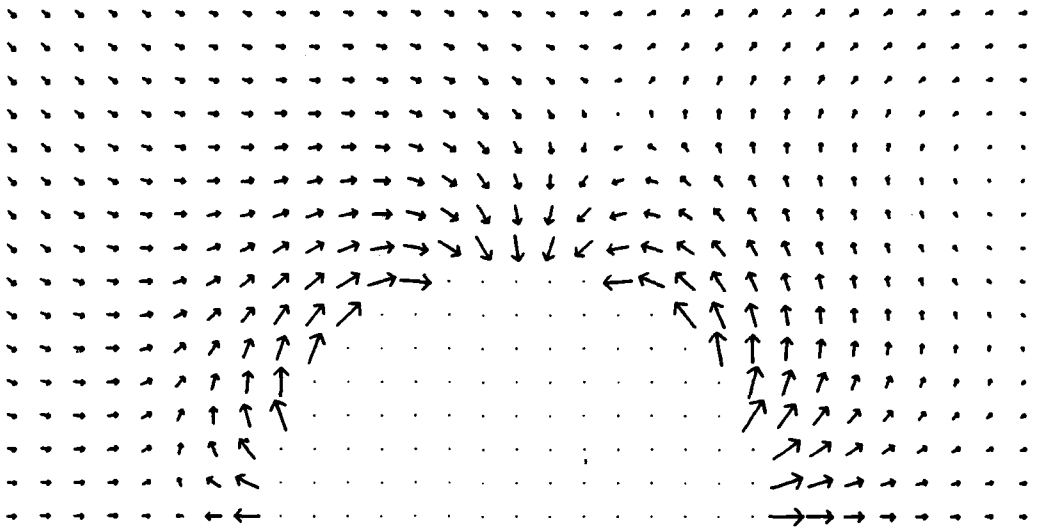

B. FREQUENCY = 342 (n=3 resonance)

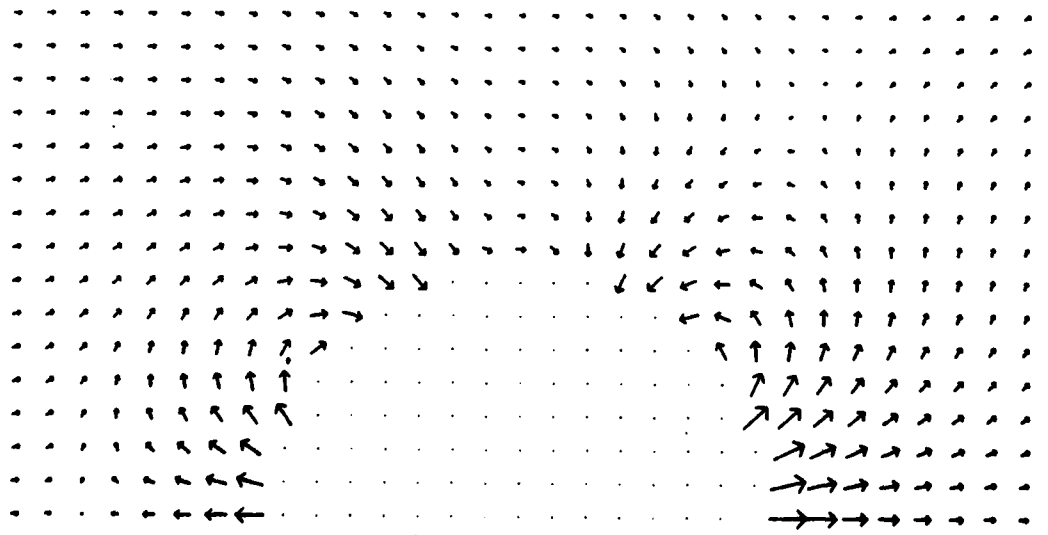

FIG.5 INTENSITY VECTORS OF THIN EMPTY SHELL

A. FREQUENCY = 788Hz (dip in spectrum)

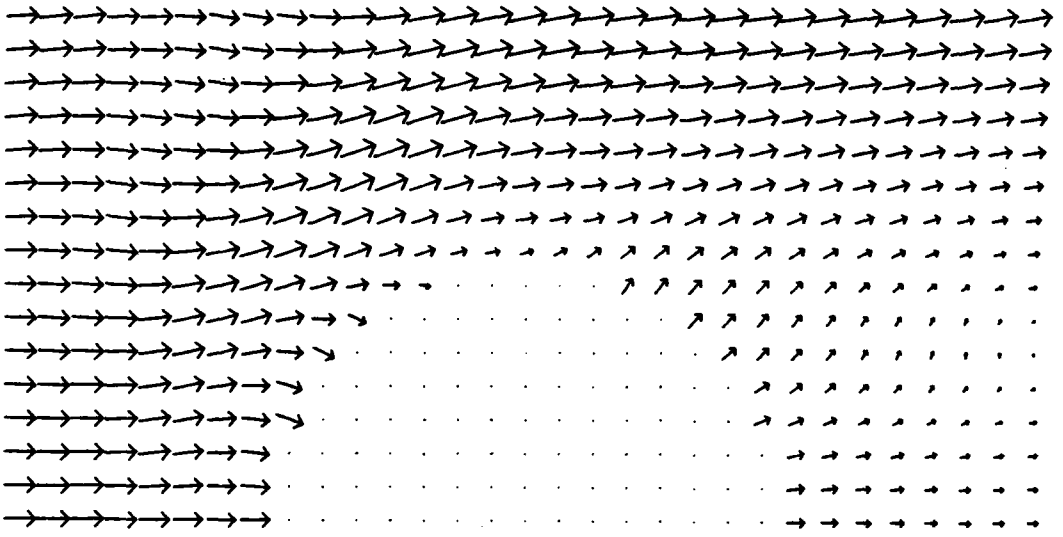

B. FREQUENCY = 1300Hz (maximum in spectrum)

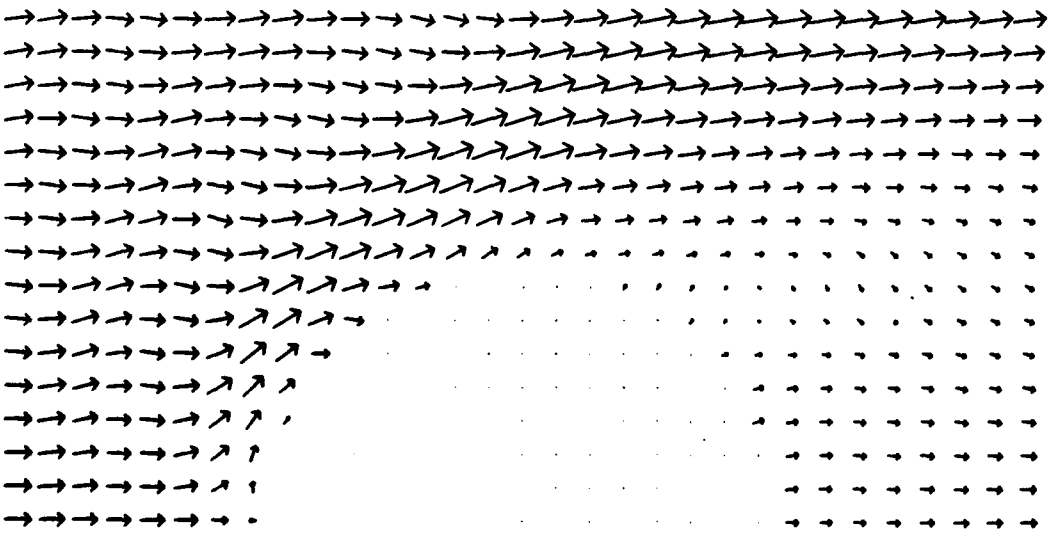

FIG.6 INTENSITY VECTORS OF THIN EMPTY SHELL

A. FREQUENCY = 194Hz (n=2 resonance)

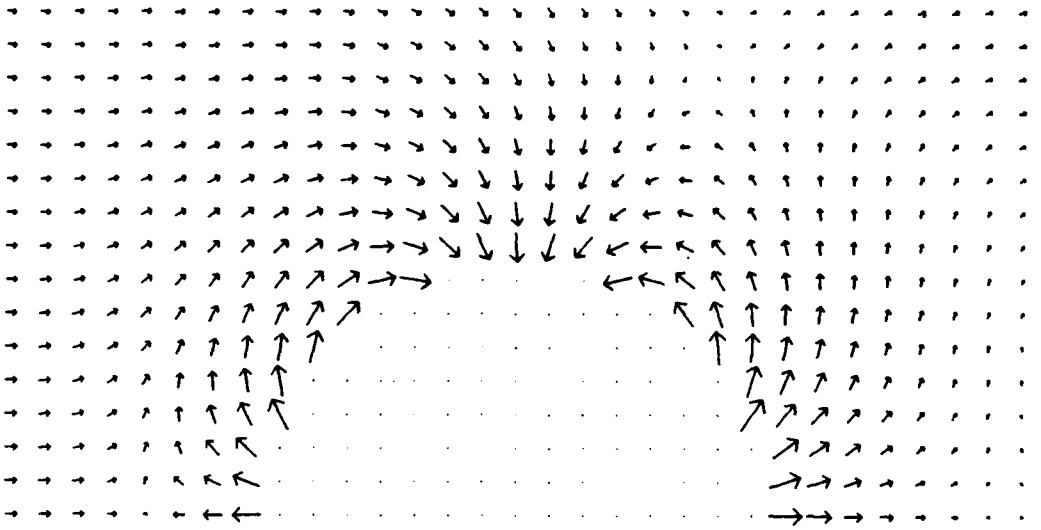

B. FREQUENCY = 175Hz (dip in spectrum)

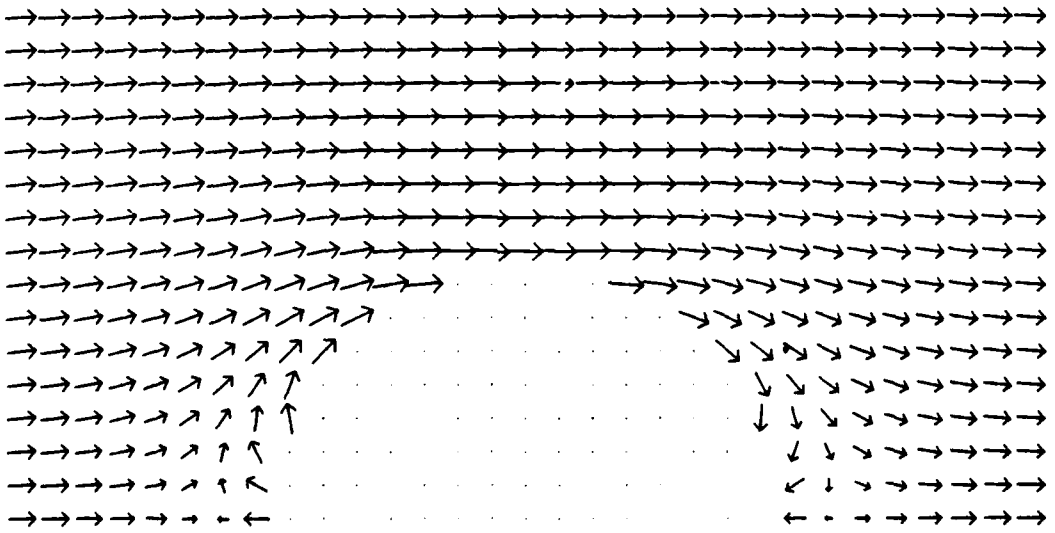

FIG.7 INTENSITY VECTORS OF THIN FLUID-FILLED SHELL

A. FREQUENCY = 497Hz (n=2 resonance)
EMPTY SHELL

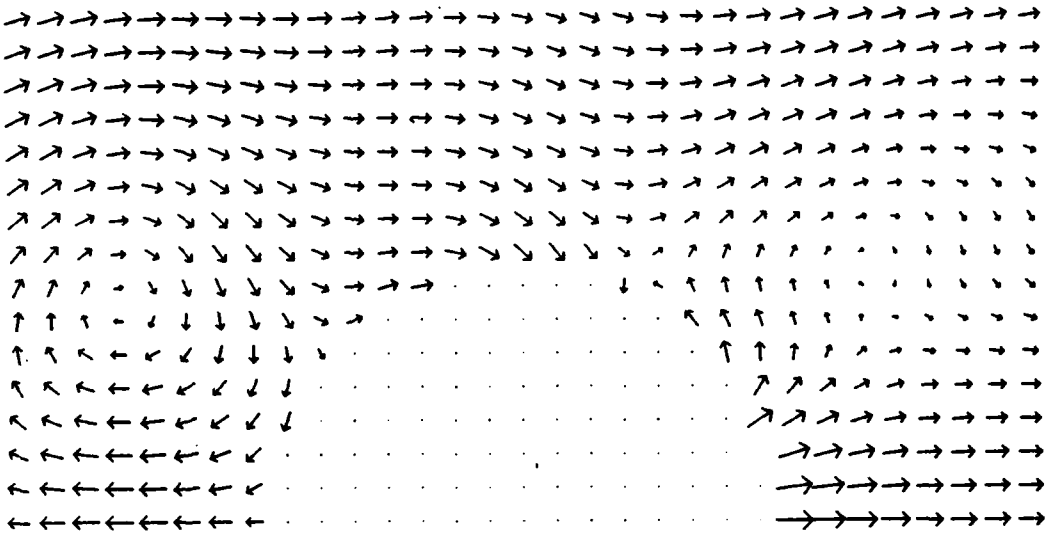

B. FREQUENCY = 556Hz (n=1? resonance)
FLUID-FILLED SHELL

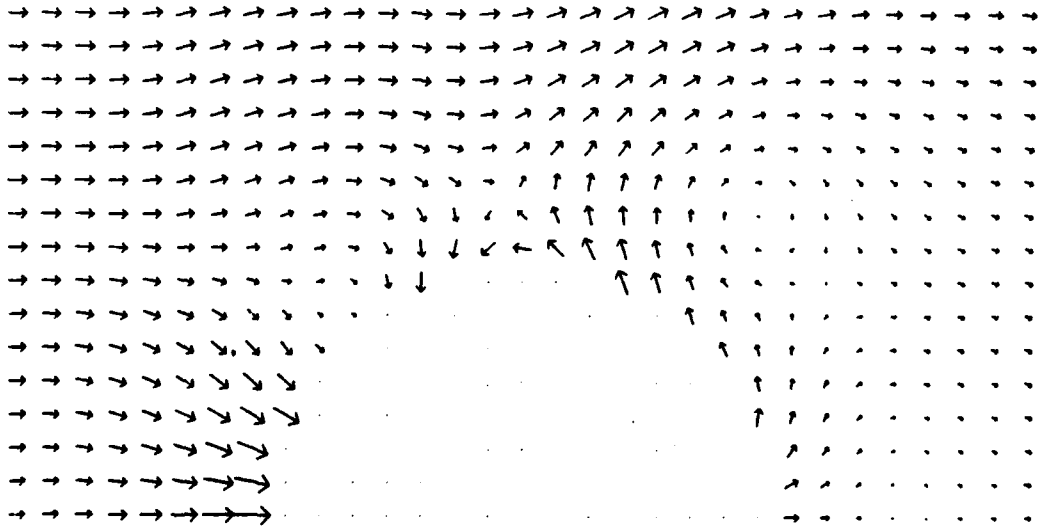

FIG.8 INTENSITY VECTORS OF THICK SHELL

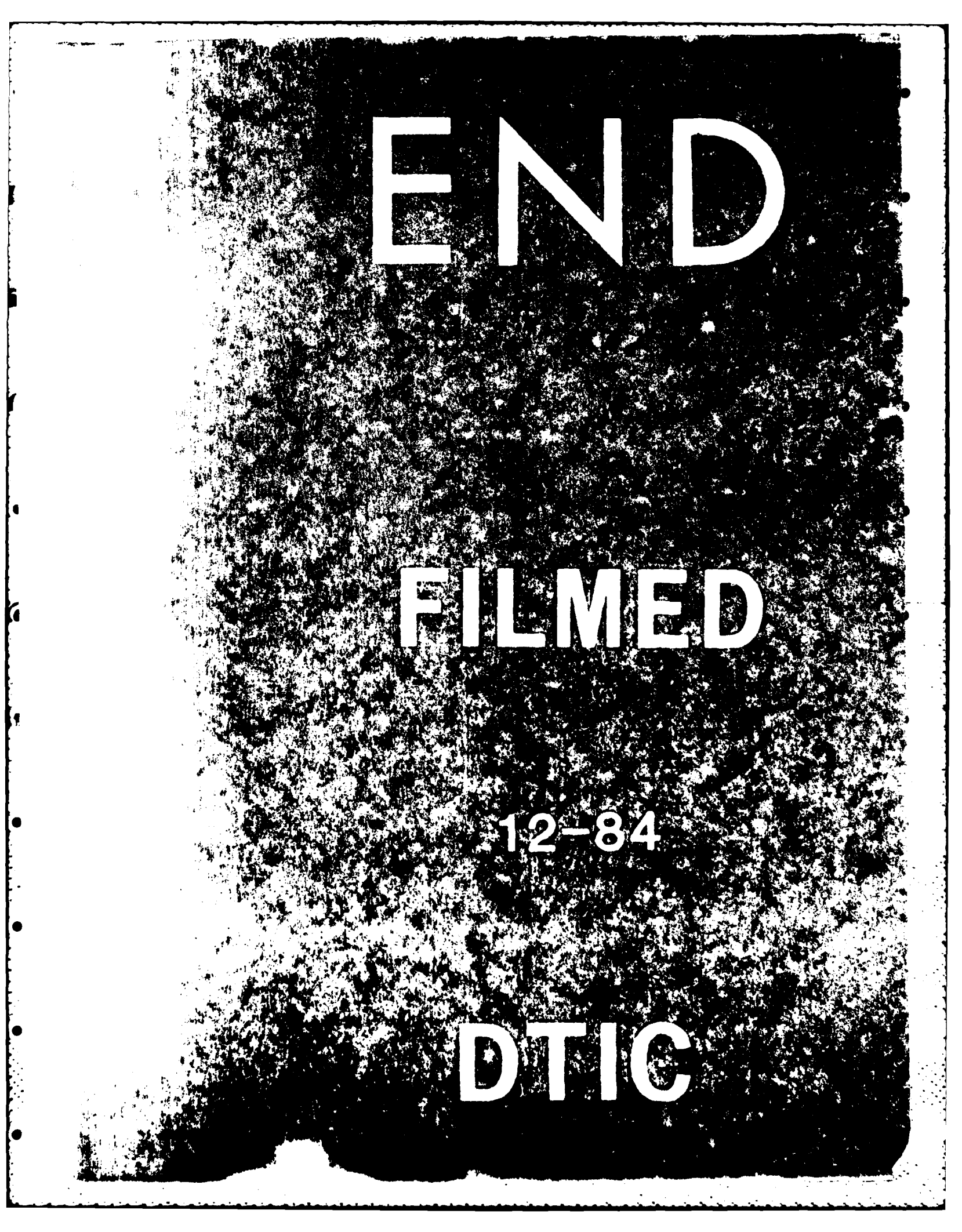
END
FILMED
12-84
DTIC